DIRECT DETERMINATION OF THE LAMELLAR STRUCTURE OF PERIPHERAL NERVE MYELIN AT MODERATE RESOLUTION (7Å)

C. R. WORTHINGTON *and* T. J. MCINTOSH

From the Departments of Biological Sciences and Physics, Carnegie-Mellon University, Pittsburgh, Pennsylvania 15213

ABSTRACT Low-angle X-ray diffraction patterns have been recorded from normal nerve and nerve swollen in glycerol solutions. The new X-ray data have a resolution of 7 Å. Direct methods of structure analysis which include deconvolution of the autocorrelation function and sampling theorem reconstructions have been used in the interpretation of the X-ray data. Phases have been assigned to the first 12 orders of diffraction from normal nerve. Fourier syntheses at a resolution of 7 Å are described and an absolute electron density scale is derived. A possible molecular interpretation of the electron density profile is given.

INTRODUCTION

Nerve myelin has been studied extensively by diffraction methods. Although low-angle X-ray diffraction was recorded as early as 1935 by Schmitt et al. (1935), the well-known pattern showing the first five orders of diffraction from peripheral nerve was first reported in 1941. The 1941 pattern (Schmitt et al., 1941) showed diffraction orders ($h = 5$) of a radial repeat distance of 170–180 Å depending on the variety of nerve. The resolution Δx of a one-dimensional Fourier synthesis is 17 Å when the first five orders are used in the synthesis. This resolution of 17 Å is called low resolution. Since 1941, many attempts (Finean and Burge, 1963; Moody, 1963; Worthington and Blaurock, 1968) have been made to solve the phase problem for the first five orders in order that a Fourier synthesis of the lamellar structure of nerve myelin at low resolution could be computed. Several accounts of these structural studies can be found in recent reviews (Finean, 1969; Worthington, 1971; Levine, 1972; Shipley, 1973; Worthington, 1973). A proof of correctness of this phase solution has now been obtained (McIntosh and Worthington, 1974). Hence, at the present time, the correct Fourier synthesis of nerve myelin at a resolution of 17 Å is known.

Higher orders of diffraction ($h \approx 12$) from a variety of peripheral nerves were first recorded in 1967–68 by Blaurock and Worthington (1969). The resolution Δx of a one-dimensional Fourier synthesis is 7 Å when the first 12 orders are used in the synthesis. This resolution is called moderate resolution. In this paper an interpretation of the lamellar structure of nerve myelin at moderate resolution is presented. It should

be mentioned that resolution better than 7 Å is possible in future work as a few very weak reflections from nerve ($h \approx 12$–18) have been recorded in some X-ray experiments (Worthington and King, 1971; Caspar and Kirschner, 1971). But these diffraction orders $h > 12$ of peripheral nerve are not considered at this time.

A few attempts have been made since 1969 to interpret the higher orders of diffraction of peripheral nerve myelin. Due to the mode of formation of the myelin sheath, the phases can only be + or −. There are a total of 2^7 or 128 different ways of assigning phases to the $h = 6$–12 orders. It is clear that there is, at present, no way of assigning phases to a peripheral nerve pattern with 12 orders of diffraction when only the one pattern is studied. Additional information is, therefore, needed in order to obtain a phase solution. In the case of the first five orders of nerve the additional information was obtained as a result of swelling experiments (Worthington and Blaurock, 1969; McIntosh and Worthington, 1974). The 1969 data from swollen nerve (Worthington and Blaurock, 1969) had about the same resolution as the first five orders of normal nerve; however, additional information relating to the first 12 orders of live nerve was not available at that time. In lieu of this experimental information, any interpretations of the higher orders of diffraction during the period 1969–72 were necessarily based upon certain assumptions. Unfortunately, the correctness of these assumptions remained uncertain.

In 1973 low-angle X-ray diffraction data from frog sciatic nerve swollen in glycerol solutions were recorded (McIntosh and Worthington, 1974), and this new X-ray data as reported here have about the same resolution as the first 12 orders of normal nerve. This swelling data provides the additional information needed to obtain the higher-order phases of nerve myelin. In this paper, direct methods of structure analysis (Worthington et al., 1973) are used to determine a set of phases for the first 12 orders of peripheral nerve myelin. The validity of this phase choice is discussed and the next most favored phase choice is also considered. A brief account of part of this work has been reported elsewhere (Worthington and McIntosh, 1973).

PREVIOUS WORK

In order that comparisons can be made between our phases (to be described) and the phases obtained by others, a brief discussion of previous work on the interpretation of the higher-order diffraction is presented. The first attempts to interpret the higher orders of diffraction from nerve were made using model-building considerations (Worthington, 1969 *a;* Worthington, 1969 *b*). The first electron density model for nerve myelin (Worthington and Blaurock, 1968) was a symmetric bilayer strip model with five parameters and this model was used to interpret the 1969 swollen nerve data and the first five orders of normal nerve. The higher-order phases of nerve myelin could have been given in 1968 from this five parameter model, but this was not done at that time for the assumption of a symmetric profile for the nerve myelin membrane at moderate resolution seemed very unlikely to be correct.[1] Accordingly, a more

[1]Worthington, C. R. Unpublished data.

TABLE I

PHASES FOR THE DIFFRACTION ORDERS h = 6–12 OF NORMAL NERVE

	$h = 6$	7	8	9	10	11	12
5-Parameter model*	+	+	−	0	+	+	+
7-Parameter model‡	+	+	−	0	−	−	−
8-Parameter model§	+	+	−	0	−	−	−
12-Parameter model§	+	+	−	0	−	−	−
Symmetric bilayer‖	+	−	+	0	+	+	−

*Worthington and Blaurock (1969).
‡Worthington (1969 *a*).
§Worthington and King (1971).
‖Caspar and Kirschner (1971).

sophisticated model for nerve was examined. This electron density model (Worthington, 1969 *b*) had seven parameters, and it indicated that the nerve myelin membrane was asymmetrical about its own center. The low-resolution Fourier synthesis of peripheral nerve (Worthington, 1971; Worthington, 1973; McIntosh and Worthington, 1974) clearly demonstrates that the nerve membrane profile is, in fact, asymmetrical. The symmetric and asymmetric electron density strip models gave quite different phases for the higher orders (h = 6–12) as shown in Table I. In later work (Worthington, 1971; Worthington and King, 1971) 8- and 12-parameter models were developed and these models had the same phases as the earlier 7-parameter model.

Additional structural information is obtained by recording other experimental points which lie on the same transform. Two sets of data which appear to have the same Fourier transform were found; these are the normal nerve pattern and the subnormal nerve pattern (Worthington and Blaurock, 1969; King, 1971; Blaurock, 1971). The sampling theorem of communication theory was used to examine these two sets of data, and this study led to a choice of a (+) phase for the sixth order of nerve (King, 1971; King and Worthington, 1971; Blaurock, 1971; Worthington, 1972). The possibility of using the sampling theorem as a method of analytic continuation was also examined (King and Worthington, 1971) but this method was later dropped as it was found that even tiny errors in the X-ray diffraction intensities can lead to quite different phase choices.

Another phase choice for the higher orders of diffraction from nerve has been given by Caspar and Kirschner (1971). These authors made two assumptions in their procedures for obtaining a structural solution. The first assumption concerned the operational procedure for limiting the possible phase choices. It was assumed that the nerve myelin membrane had an approximate center of symmetry, and the distance u of the membrane center to the cytoplasmic boundary was determined. The possible phase choices were then obtained by dividing the sampled transform by the centrosymmetric fringe function $\cos 2\pi hu/d$ (see Fig. 3 *c* of Casper and Kirschner, 1971). In order to obtain a phase solution, it was also assumed that the structure of rabbit sciatic nerve was the same as rabbit optic nerve. It has been argued that these two assumptions of Caspar and Kirschner are incorrect (Worthington, 1973). We note that the operational

procedure of dividing by the centrosymmetric fringe function is valid only if the nerve myelin membrane has an exact center of symmetry. The low-resolution Fourier synthesis of nerve (Worthington, 1971; Worthington, 1973; McIntosh and Worthington, 1974) shows that the nerve myelin membrane does not have a symmetrical profile. Moreover, the assumption that sciatic and optic nerves have the same structure is contradicted by differences in chemical composition. Differences in the lipid composition of sciatic and optic nerves have been found (O'Brien, 1967; Eng et al., 1968). It is now well established that the protein composition of sciatic and optic nerves is considerably different (Eng et al., 1968; London, 1971; Greenfield et al., 1973; Eylar, 1973). In earlier X-ray studies structural differences between sciatic and optic nerves were apparent from either examining Fourier syntheses at low resolution using the X-ray data of Worthington and Blaurock (1969) or from model-building considerations (Worthington, 1969 *a*). Nevertheless, by using these assumptions, Caspar and Kirschner (1971) obtained the surprising result that the hydrocarbon chain region of rabbit sciatic nerve is wider than the corresponding region of frog sciatic nerve by 3 Å. This is at variance with the results of model-building for it was found that rabbit (and rat) sciatic nerves have hydrocarbon regions of the same size as frog sciatic nerve (Worthington, 1969 *b;* King, 1971). It can be seen from Table I that the phases obtained by Caspar and Kirschner (1971) resemble the phases of the five-parameter model, and it follows that the two Fouriers are somewhat similar (Worthington, 1972).

In summary, the phases listed in Table I for orders $h = 6$–12 have been obtained in previous work. In each case, these phases were deduced on the basis of certain assumptions. It would appear that the nerve membrane profile is not exactly symmetrical about its center and hence the phases given by the five-parameter model (Worthington and Blaurock, 1969) and the phases given by Caspar and Kirschner (1971) are suspect. On the other hand, the phases given by the later models (Worthington, 1969 *a;* Worthington and King, 1971) are not disproved, but a proof of correctness has not been obtained.

METHODS

Low-angle X-ray diffraction patterns were obtained from frog *Rana pipiens* sciatic nerves. X-ray patterns were obtained from nerves in Ringer's solution (Long, 1961; see p. 58), pH = 7.3, or from nerves swollen in glycerol solutions. All exposures were taken at room temperature. The same procedures and experimental methods were used as described previously (McIntosh and Worthington, 1974). The only difference was that the X-ray exposure times were slightly longer so as to record the higher orders of diffraction, but exposure times usually did not exceed 12 h. Low-angle X-ray diffraction patterns were also obtained from rabbit sciatic nerves.

DIFFRACTION THEORY

The structure analysis of the low-angle X-ray diffraction data as used in this paper follows that of a previous paper (McIntosh and Worthington, 1974). The diffraction

theory has also been given elsewhere (Worthington, 1969 *b;* Worthington, 1971; King and Worthington, 1971; Worthington et al., 1973). Thus only a summary of the notation and equations is presented here.

Let $t(x)$ represent the electron density distribution in the radial direction of a single unit cell, and let $T(X)$ represent its Fourier transform, where x, X are real and reciprocal phase coordinates. Nerve myelin has a multilayered assembly so that discrete reflections are recorded at $X = h/d$, where h is an integer. Integrated intensities $I(h)$ are measured but corrected intensities $J_{obs}(h) = hI(h)$ are used in the X-ray analysis. Any two sets of X-ray data are placed on the same relative scale using the formula of Worthington and Blaurock (1969). The notation $J(h) = |T(h)|^2$ and $J(h) = KJ_{obs}(h)$ is retained, where K is the normalization constant. It is convenient to assume $K = 1$ until an absolute scale is considered when a precise value is assigned to K.

A model for $t(x)$ is considered which contains an extracellular fluid space. Let the membrane pair have electron density $m(x)$, and F is the electron density of the fluid layer. The origin of the unit cell is at the center of the membrane pair. The unit cell has a center of symmetry at the origin. The membrane pair has average electron density M and width v, while the fluid layer has width $d - v$. The minus fluid model $\Delta t(x)$ is defined, where $\Delta t(x) = t(x) - F$. The membrane pair then has electron density $m(x) - F$, and the space $d - v$ has zero electron density.

The Fourier transform of $\Delta t(x)$ is denoted $\Delta T(X)$ and

$$\Delta T(X) = T(X) - Fd\,\mathrm{sinc}\,\pi dX, \tag{1}$$

where $\mathrm{sinc}\,\theta = \sin\theta/\theta$. Hence, $\Delta T(h) = T(h)$, provided that h is a non-zero integer. Thus, the two models, $t(x)$ and $\Delta t(x)$, cannot be distinguished on the basis of the low-angle X-ray data as the $h = 0$ reflection is not observed.

The Fourier series representation for both models is

$$(2/d)\sum_{1}^{h}\{\pm\}\,|T(h)|\cos 2\pi hx/d, \tag{2}$$

where $\{\pm\}$ is the phase information. The Patterson function for both models is

$$(2/d)\sum_{1}^{h}J(h)\cos 2\pi hx/d. \tag{3}$$

The additional information needed to solve the phase problem is obtained from swelling experiments. Let $M(X)$ denote the Fourier transform of $m(x)$. The Fourier transform $\Delta T(X)$ for the minus fluid model is

$$\Delta T(X) = M(X) - Fv\,\mathrm{sinc}\,\pi vX. \tag{4}$$

Discrete X-ray reflections occur at $X = h/d$, h an integer. In another experiment using

the same fluid F, the unit cell size might change from d to D so that discrete reflections occur at $X = H/D$, H an integer. If no change in $m(x)$, v, or F occurs, then the two sets of data $\Delta J(h)$ and $\Delta J(H)$ lie on the same intensity transform $\Delta J(X)$. Knowledge of $\Delta J(X)$ is, therefore, obtained as a result of swelling experiments.

The direct methods of structure analysis referred to in this paper are deconvolution and reconstruction methods. The deconvolution methods are based upon the original theory of Hosemann and Bagchi (1962), while the reconstruction methods are based on the sampling theorem of communication theory (Shannon, 1949).

Deconvolution

The deconvolution method refers to a deconvolution of the autocorrelation function $\Delta A(x)$, where

$$\Delta A(x) = \Delta t(x) * \Delta t(-x), \tag{5}$$

and where $*$ is the convolution symbol. The autocorrelation function $\Delta A(x)$ is obtained from a Fourier transformation of the continuous intensity transform $\Delta J(X)$. $\Delta A(x)$ can be deconvoluted to give an n-strip electron-density model for $\Delta t(x)$, but two solutions $\pm\Delta t(x)$ are obtained (Hosemann and Bagchi, 1962; Worthington et al., 1973). Deconvolution can be carried out using either the recursion or the relaxation method. The recursion method has been previously used in determining the structure of model membrane systems (Lesslauer et al., 1972) and of retinal photoreceptors (Worthington, 1973). However, the recursion method does not work for nerve myelin (McIntosh and Worthington, 1974), and the relaxation method, therefore, is used.

In the relaxation method, an n-strip model $s(x)$ is proposed as a solution. The autocorrelation function $s(x) * s(-x)$ is calculated and compared with the observed $\Delta A(x)$ via a residual function $R(x)$, where

$$R(x) = \Delta A(x) - s(x) * s(-x). \tag{6}$$

The solution $s(x)$ is varied until $R(x)$ is minimized. The actual minimization is obtained using the conjugate gradient method (Fletcher and Reeves, 1964). A systematic procedure is used in order to examine each possible phase choice. If there are r possible phase choices, then there are r different trial solutions $s(x)$ and r different residual functions $R(x)$. An initial solution or model $s(x)$ is first obtained from the Fourier synthesis corresponding to that particular phase choice. The $(\pm)$ phase choice which gives the lowest $R(x)$ is the correct one.

Reconstruction

The appropriate expression for a reconstruction of $\Delta T(X)$ is

$$\Delta T(X) \approx \sum_{-h}^{h} \{\pm\} \, |\, \Delta T(h) \,|\, \operatorname{sinc}(\pi dX - \pi h). \tag{7}$$

A finite number of orders are used in the summation. The expression in Eq. 7 contains the $\Delta T(0)$ term, which is not recorded experimentally. A value for $\Delta T(0)$ is obtained using the procedure of King and Worthington (1971).

Consider two sets of X-ray data $T(h)$ and $T(H)$ which lie on the same intensity transform $\Delta J(X)$. The data sets $J(h)$ and $J(H)$ have repeat distances d and D, respectively. The continuous transform $\Delta T(X)$ is computed from Eq. 7 using the $|\Delta T(h)|$ values from the $J(h)$ data set and using all phase possibilities. If there are r possible phase choices, then there are r different reconstructed transforms. The phase choice which generates a continuous transform consistent with the other data set $J(H)$ is the correct phase choice. However, there is one ambiguity in that the correct phase choice and the exactly opposite phase cannot be distinguished by this method.

RESULTS

Low angle X-ray diffraction data from frog sciatic nerve swollen in glycerol solutions have been recorded. This X-ray data from swollen nerve have about the same resolution as the first 12 orders of normal nerve. It is known from previous work (McIntosh and Worthington, 1974) that the molecular structure of the membrane pair remains uneffected by swelling in glycerol solutions provided that the concentration of the glycerol solution does not exceed 20%. A series of X-ray experiments was performed using 0%, 6.5%, and 15% glycerol. In particular, many experiments were run using 6.5% glycerol as 6.5% glycerol has the same electron density as Ringer's solution.

Typical densitometer traces of X-ray patterns of live frog sciatic nerve and of swollen frog sciatic nerve are presented in Figs. 1 A and B. Reproductions of these X-ray patterns at low resolution (17 Å) have been shown by McIntosh and Worthington (1974), while reproductions of the higher-order reflections of live frog sciatic nerve have been previously shown by Blaurock and Worthington (1969). It is evident from Fig. 1 A that the higher-order reflections of normal nerve become broader with increase in diffraction order but orders $h = 1$ to 12 can be distinguished. In the case of swollen nerve, the reflections become broader even at low resolution (17 Å), while the higher orders overlap each other and occur as diffuse reflections. The procedure for measuring the diffuse reflections and the theoretical aspects of this procedure are presented in Appendix I. In summary, the integrated intensities of the lower orders of the swollen nerve pattern are obtained by measuring the area under the densitometer tracing belonging to that reflection. The X-ray intensities of the diffuse reflections are obtained by using the sampling period (d) of the lower-order reflections and by measuring the area under the densitometer tracing for that sampling interval (h/d). In this way a set of integrated intensities are obtained for each swelling experiment. Different sets of X-ray data are then placed on the same relative scale. This procedure enables the different data sets to be presented visually, and it will be demonstrated that experimental data points obtained in different experiments all lie on the same Fourier transform curve. We note that Levine and Wilkins (1971) and Lesslauer et al. (1972) in the study of model membrane systems have made comparisons between the discrete reflections from multilayers and the continuous diffraction from dispersions.

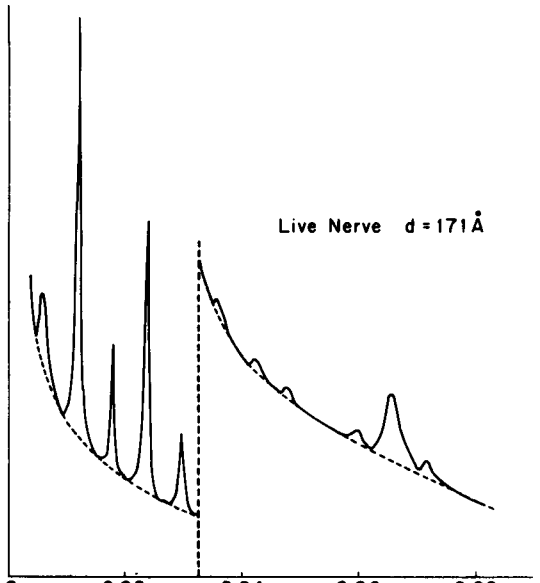

FIGURE 1A

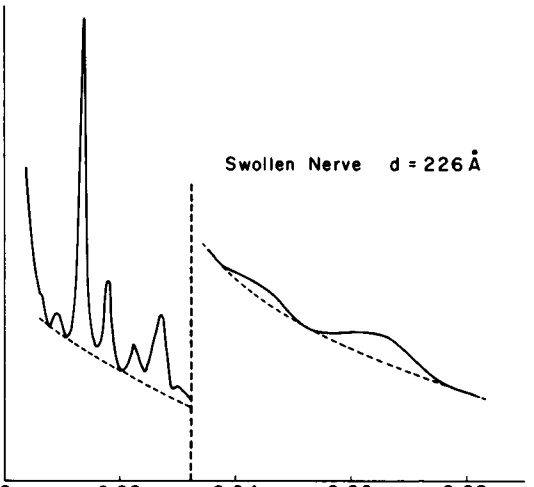

FIGURE 1B

FIGURE 1 A Densitometer tracing of diffracted intensity as a function of reciprocal spacing X. The low-resolution tracing where $X < 0.032$ Å^{-1} was obtained using a shorter exposure than the moderate-resolution tracing where $X > 0.032$ Å^{-1}. The low-resolution tracing shows the first five orders of diffraction from frog sciatic nerve in Ringer's solution, $d = 171$ Å. The low orders are sharp and all lie on a smooth background curve. The higher orders $h = 6$–12 are clearly separate and again all lie on a continuous background curve.

FIGURE 1 B Densitometer tracing of diffracted intensity as a function of reciprocal spacing X. The low-resolution tracing where $X < 0.032$ Å^{-1} was obtained using a shorter exposure than the moderate-resolution tracing where $X > 0.032$ Å^{-1}. The low-resolution tracing shows discrete orders of diffraction from frog sciatic nerve swollen in 0% glycerol, $d = 226$ Å. The moderate-resolution tracing shows two diffuse reflections centered at $X = 0.044$ Å^{-1} and at $X = 0.065$ Å^{-1}. Note that the diffraction orders $h = 7$ and 8 of live nerve fall within the region of the diffuse reflection centered at $X = 0.044$ Å^{-1} and orders $h = 10$, 11, and 12 of live nerve fall within the region of the diffuse reflection centered at $X = 0.065$ Å^{-1}.

The low-angle X-ray data from frog sciatic nerve in 0%, 6.5%, and 15% glycerol solutions are plotted in Figs. 2, 3, and 4, respectively. The repeat periods of the swollen patterns vary from $d = 190$ Å to $d = 270$ Å and no attempt has been made to identify different data sets when using the same glycerol concentration. The swollen nerve data $|T(h)|$ values are identified as small black dots and are plotted out to reciprocal spacing values of 0.075–0.078 Å^{-1} (which corresponds to a minimum spacing of about 13 Å). In each case, the swollen nerve data points trace out a continuous curve, and this curve, which is shown as a dotted line, has been drawn in by eye. There are six separate peaks I, II, III, IV, V, and VI in each of the continuous curves in Figs. 2–4. Note that region IV has very weak intensity in Figs. 2 and 4 and is not as well-defined as the other peaks. These continuous curves are not the same for, from the *Fv*

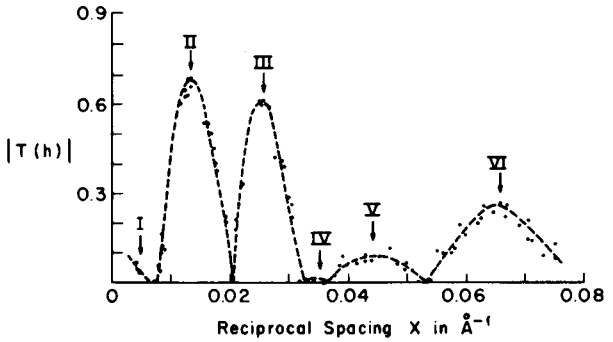

FIGURE 2 Low-angle X-ray diffraction data from nerve myelin swollen in water. The Fourier transform values are represented by small black dots (·) and are plotted vs. reciprocal space coordinate X. The continuous transform (dotted line) has been drawn in by eye, and regions I, II, III, IV, V, and VI of the transform are indicated.

sinc $\pi\nu X$ term in Eq. 4, the diffracted amplitude is dependent on the fluid density. The sinc term, however, only has noticeable effect on the curve for values of $X \leq 0.04$ Å^{-1}. Thus, the peaks I–IV in Figs. 2–4 show differences, whereas peaks V and VI in Figs. 2–4 are very similar in shape.

The $|\,T(h)\,|$ data points for frog sciatic nerve in Ringer's solution are identified as large open circles and are plotted in Fig. 3, together with the data points from nerve swollen in 6.5% glycerol. The X-ray data from normal nerve fit very nicely on the Fourier transform of the nerve swollen in 6.5% glycerol. From Eq. 4 it follows that the molecular structure of the membrane pair is the same for both the normal nerve and nerve swollen in 6.5% glycerol. It is appropriate to note that frog sciatic nerve data reported by Casper and Kirschner (1971) do not lie on the curve shown in Fig. 3. The reason for this discrepancy is not known but differences in densitometer tracings are

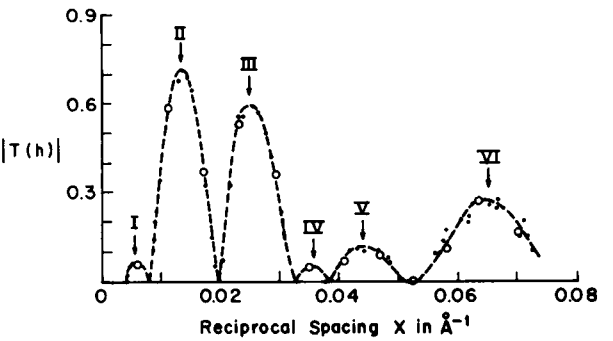

FIGURE 3 Low-angle X-ray diffraction data from normal nerve myelin in Ringer's solution (d = 171 Å) and nerve myelin swollen in 6.5% glycerol (d = 190–260 Å). The Fourier transform values $|\,T(h/d)\,|$ are plotted vs. reciprocal space coordinate X. The Fourier transform values of normal nerve are indicated by open circles (o), while the Fourier transform values of swollen nerve are indicated by small black dots (·). The continuous transform (dotted line) has been drawn in by eye, and regions I, II, III, IV, V, and VI of the transform are indicated.

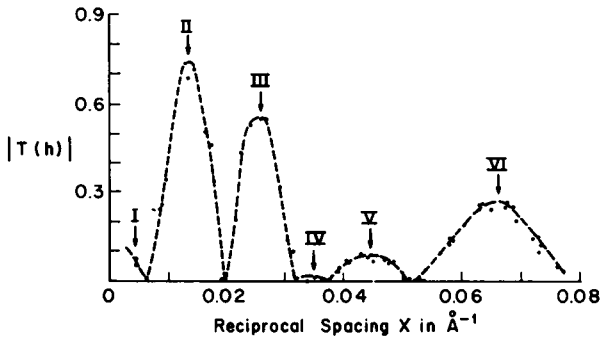

FIGURE 4 Low-angle X-ray diffraction data from nerve myelin swollen in 15% glycerol. The Fourier transform values are represented by small black dots (·) and are plotted vs. reciprocal space coordinate X. The continuous transform (dotted line) has been drawn in by eye, and regions I, II, III, IV, V, and VI of the transform are indicated.

apparent. Our tracings in Fig. 1 A show that the diffraction orders from live nerve all lie on smooth background curves, and the area associated with each reflection has been measured. On the other hand, the Caspar and Kirschner (1971) tracings show uneven background curves.

INTERPRETATION

The continuous curves in Figs. 2–4 define six separate regions in the Fourier transform. Each region can be $\{\pm\}$ and there are a total of 2^6 possible phase choices. However, the phases of regions I–III are known to be $(-, +, -)$ from previous work (McIntosh and Worthington, 1974), so that only the phases of regions IV–VI are unknown. There are 2^3 possible phase choices for regions IV–VI. The normal nerve pattern has the $h = 6$ order in region IV, the $h = 7, 8$ orders in region V and the $h = 10, 11, 12$ orders in region VI. The $h = 9$ order of normal nerve occurs at a minima between regions V and VI and this reflection is estimated to have zero intensity. If the $h = 6$–8, 10–12 orders of diffraction of the normal pattern were considered separate from the swelling data, then there are $2^6 = 64$ phase possibilities for the higher orders of normal nerve. The swelling data in Figs. 2–4 simplifies the phase problem of the higher-order diffraction from 64 choices to 8 phase choices.

The direct methods of structure analysis when applied to the swelling data of nerve give the correct phases but there is a $(\pm)$ ambiguity. Thus, if the direct methods were applied to regions I–VI, then two solutions $\pm\ \Delta t(x)$ are obtained. But the $(\pm)$ ambiguity has been resolved for the first three regions (McIntosh and Worthington, 1974) so that the correct set of phases for regions I–III are already known. Thus, according to diffraction theory, the direct methods when applied to regions IV–VI provide the correct set of phases for these three regions. The direct methods refer to deconvolution and reconstruction methods.

Deconvolution Results

The autocorrelation function $\Delta A(x)$ can be obtained as a result of a Fourier transformation of the X-ray data. It was originally hoped that the swelling data would have a repeat period $d \geq 2v$, where v is the width of the membrane pair, for in this case $\Delta A(x)$ can be obtained directly from the Patterson function using one set of data (Worthington et al., 1973). However, the observed repeat distances of swollen nerve were in the range of d = 190 Å to d = 270 Å and as v was likely to be about 160 Å (Worthington, 1972) another method was used. A fictitious period of d = 360 Å was chosen and transform values at intervals of h/d were obtained from the continuous curves in Figs. 2–4 and Patterson functions were computed using Eq. 3. The transform values for the higher-order diffraction where $0.032\ \text{Å}^{-1} \leq X \leq 0.080\ \text{Å}^{-1}$ are known as the continuous intensity transform is directly recorded (see Fig. 1 B and Appendix). The transform values for the lower-order diffraction where $X \leq 0.032\ \text{Å}^{-1}$ are obtained as a result of recording many sets of X-ray data from nerves swollen in 0%, 6.5%, and 15% glycerol, each data set contains a series of discrete reflections (see Fig. 1 A and Appendix). Only a few of these data sets have been plotted in Figs. 2–4. The additional data sets have been previously shown (McIntosh and Worthington, 1974) (see Figs. 4 A, 3, and Fig. 4 B, pp. 370 and 371) and it is noted that, although many data points are clustered together, there are also data points which are distributed throughout the low-angle region. Thus, the continuous Fourier transform curves for $X \leq 0.032\ \text{Å}^{-1}$ were effectively traced out and could be accurately drawn in by eye. We note that the precision of the continuous Fourier transform (modulus) for nerve swollen in 6.5% glycerol has been demonstrated by comparison with the continuous transform curve which was computed from the sampling theorem (McIntosh and Worthington, 1974) (see Fig. 7 A, p. 377).

The autocorrelation function $\Delta A(x)$ is obtained from the Patterson function by shifting the base line of the Patterson such that $\Delta A(v) = 0$. The actual value of v is the value of the radial distance x, where the Patterson function levels off and is parallel to the x-axis. A value of v = 160 Å was obtained. The autocorrelation function $\Delta A(x)$ for nerve swollen in 6.5% glycerol and normal nerve is shown in Fig. 5. $\Delta A(x)$ was obtained from the Patterson function of the X-ray data in Fig. 3, using d = 360 Å and by shifting the base line so that $\Delta A(160) = 0$. The autocorrelation functions $\Delta A(x)$ for nerve in 0% and 15% glycerol were obtained in a similar way. The question of whether the autocorrelation function does level off for $x > v$ has been verified (McIntosh and Worthington, 1974) by computing $\Delta A(x)$ using a larger period of d = 500 Å and noting that $\Delta A(x)$ was essentially zero for $x > v$.

The choice of v in the recursion method is of critical importance. On the other hand, the choice of v is not a critical factor in the relaxation method as a small tolerance of ±5 Å leads to very similar results (McIntosh and Worthington, 1974). The correctness of our choice of v, the membrane pair width, can be examined by computing the Fourier transform of the autocorrelation function but using the integration limits of

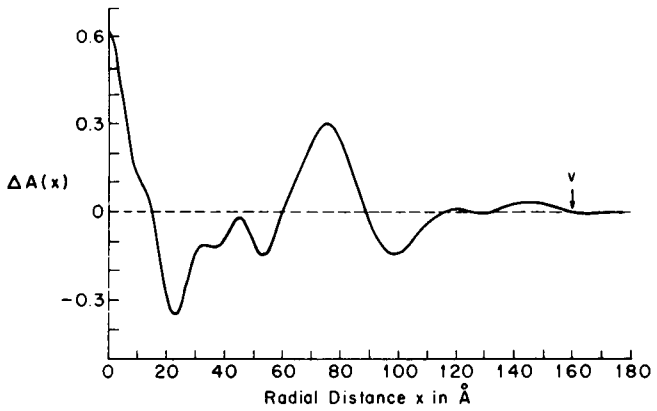

FIGURE 5 The autocorrelation function $\Delta A(x)$ for a single unit cell of nerve myelin. The membrane pair width ν = 160 Å is indicated by an arrow.

0 to ν instead of 0 to ∞. If ν is correctly chosen then

$$\Delta J(X) = 2 \int_0^{\nu} \Delta A(X) \cos 2\pi X x \, dx. \tag{8}$$

The continuous intensity transform $\Delta J(X)$ was computed using the $\Delta A(x)$ curve of Fig. 5 and using ν = 160 Å. This calculated transform curve $\Delta J(X)$ together with the 6.5% glycerol and normal nerve data points are shown in Fig. 6. The experimental data points fit very closely to the calculated curve and hence it follows that the choice of ν = 160 Å is quite accurate. The close fit of the experimental data to the calculated curve also implies that $\Delta A(x)$ as shown in Fig. 5 is a precise representation of the autocorrelation function of the unit cell.

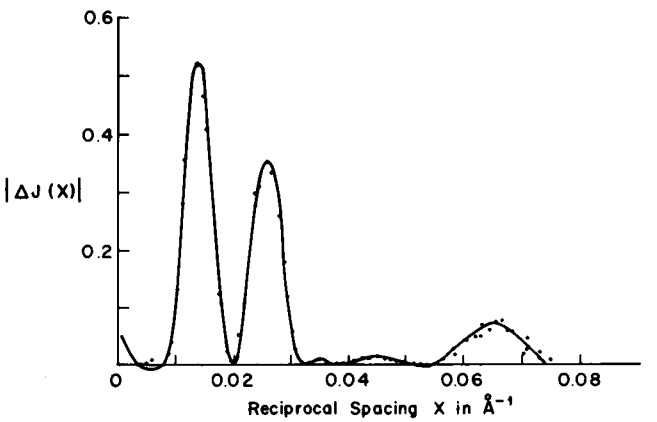

FIGURE 6 The continuous intensity curve $\Delta J(X)$ plotted vs. reciprocal space coordinate X. The theoretical curve (solid line) was computed from Eq. 8 with ν = 160 Å. The experimental intensities are represented by small black dots (·).

TABLE II

AI VALUES FOR EACH PHASE CHOICE IN REGIONS IV, V, AND VI

Regions:	Phases IV	V	VI	Glycerol:	AI values 0%	6.5%	15%
					%	%	%
	+	−	−		6.0	5.1	4.9
	+	−	+		6.6	5.9	5.4
	+	+	−		6.7	6.0	5.7
	+	+	+		6.5	6.2	5.5
	−	−	−		6.0	5.7	4.9
	−	−	+		6.6	5.9	5.4
	−	+	−		6.7	6.0	5.7
	−	+	+		6.5	6.2	5.5

The deconvolution of $\Delta A(x)$ for the 0%, 6.5%, and 15% glycerol data was carried out using a uniform strip model where the strips were 4 Å wide and where ν = 160 Å was used. The residual function $R(x)$ defined by Eq. 6 is expressed in terms of an agreement index AI where

$$\text{AI} = \frac{\Sigma \mid R(x) \mid}{\Sigma \mid \Delta A(x) \mid} (100\%). \tag{9}$$

The AI values for the various phase choices for regions IV–VI for the three sets of X-ray data are listed in Table II. Eight phase choices are examined using the 6.5% glycerol and normal nerve data. However, in case of the 0% and 15% glycerol data, region IV has very weak intensity so that only the phase choices for regions V and VI are examined.

The phase choice (−, −) for regions V and VI has the lowest AI values for the three sets of X-ray data shown in Figs. 2–4. The phase choice (+) for region IV has the lowest AI value for the 6.5% glycerol and normal nerve data. Thus, if it can be assumed that differences in AI values are significant, then the results of the deconvolution indicate that the correct phase choice for regions IV–VI is (+, −, −).

Reconstruction Results

The sampling theorem expression of Eq. 7 can be used as a method of phase determination for regions IV–VI of Fig. 3. The procedure is to reconstruct the continuous Fourier transform $\Delta T(X)$ for normal nerve using the eight phase choices for regions IV–VI together with the known phases (−, +, −) for regions I–III. There are eight different reconstructions, one for each phase choice. The reconstructed Fourier transform $\Delta T(X)$ with the correct phase choice will provide the best match with the 6.5% glycerol data. The sampling theorem analysis is carried out in two stages. First, the phase of region IV is examined and, after the phase of region IV has been established, the phases of regions V and VI are studied.

The reconstructed Fourier transform $\Delta T(X)$ is calculated for normal nerve using

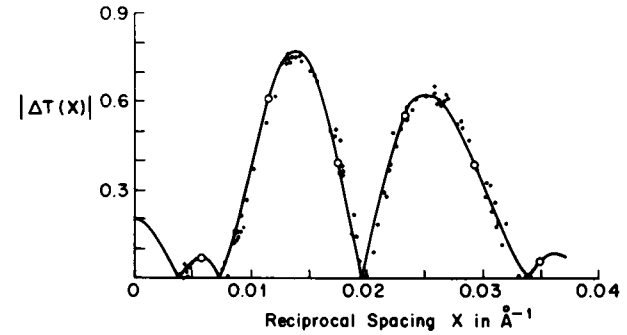

FIGURE 7 The modulus of the continuous transform $|\Delta T(X)|$ plotted vs. reciprocal space coordinate X. The $|\Delta T(X)|$ curve (solid line) was computed using the sampling theorem and normal data, d = 171 Å, with phases (−, +, −, +) for regions I, II, III, and IV of the transform. The Fourier transform values of normal myelin are indicated by open circles (o), while the corresponding values for myelin swollen in 6.5% glycerol are indicated by small black dots (·).

either a (+) or a (−) phase for region IV and the known phases (−, +, −) for regions I–III. The continuous transform $\Delta T(X)$ is computed from Eq. 7 using the first six orders of diffraction of d = 171 Å from frog sciatic nerve as well as the zero-order term $\Delta T(0)$. The value of $\Delta T(0)$ had been found in previous work (McIntosh and Worthington, 1974). The continuous transform curves $|\Delta T(X)|$ together with the normal nerve data (open circles) and the 6.5% glycerol data (small black dots) are shown in Figs. 7 and 8. The $|\Delta T(X)|$ curve in Fig. 7 has a (+) phase whereas the $|\Delta T(X)|$ curve in Fig. 8 has a (−) phase. Note that the normal nerve data lies exactly on both the $\Delta T(X)$ curves as required by the computation. It is seen that the experimental data points (small black dots) lie much closer to the $|\Delta T(X)|$ curve in Fig. 7 and hence the correct phase for region IV is (+).

The reconstructed Fourier transform $\Delta T(X)$ is calculated for normal nerve using

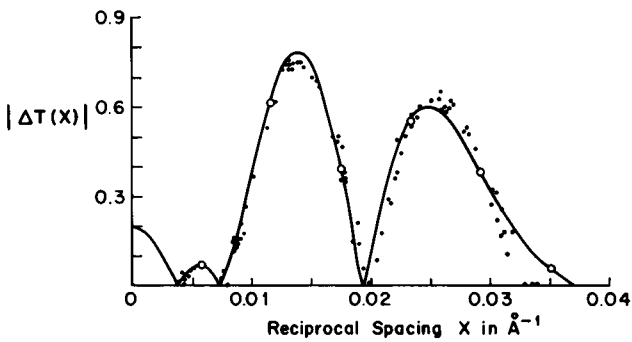

FIGURE 8 The modulus of the continuous transform $|\Delta T(X)|$ plotted vs. reciprocal space coordinate X. The $|\Delta T(X)|$ curve (solid line) was computed using the sampling theorem and normal data, d = 171 Å, with phases (+, +, −, −) for regions I, II, III, and IV of the transform. The Fourier transform values of normal myelin are indicated by open circles (o), while the corresponding values for myelin swollen in 6.5% glycerol are indicated by small black dots (·).

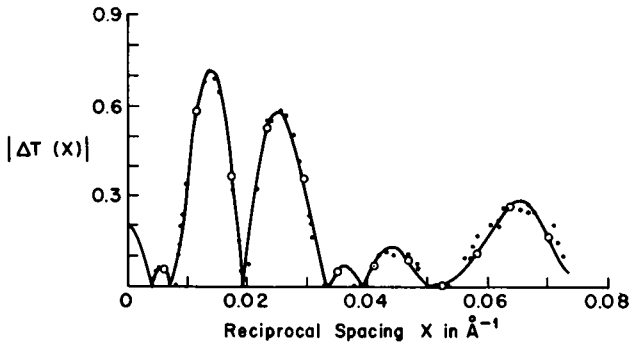

FIGURE 9 The modulus of the continuous transform $|\Delta T(X)|$ plotted vs. reciprocal space coordinate X. The $|\Delta T(X)|$ curve (solid line) was computed using the sampling theorem and normal data, d = 171 Å, with phases (−, +, −, +, −, −) for regions I, II, III, IV, V, and VI. The Fourier transform values of normal myelin are indicated by open circles (o), while the corresponding values for myelin swollen in 6.5% glycerol are indicated by small black dots (·).

the four phase choices for regions V and VI and the known phases (−, +, −, +) for regions I–IV. The transform is computed from Eq. 7 using h = 12 orders of diffraction of d = 171 Å from frog sciatic nerve as well as the zero-order term $\Delta T(0)$. The continuous curves $|\Delta T(X)|$ together with the normal nerve data (open circles) and the 6.5% glycerol data (small black dots) are shown in Figs. 9–12. The curves in Figs. 9–12 have phases (−, −), (−, +), (+, −), and (+, +) for regions V and VI, respectively.

In order to compare the matching of the data points quantitatively, it is convenient to define R-equivalent (RE) as follows:

$$\mathrm{RE} = \frac{\Sigma \big| \, |\Delta T(h)| - |T(h)| \, \big|}{\Sigma |T(h)|}(100\%), \tag{10}$$

where $T(h)$ refers to the observed data points in Figs. 9–12, $\Delta T(h)$ refers to the

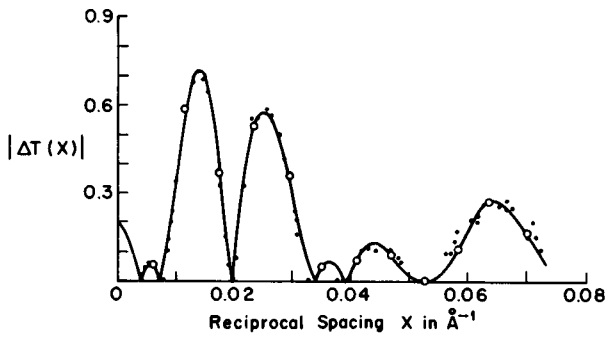

FIGURE 10 The modulus of the continuous transform $|\Delta T(X)|$ plotted vs. reciprocal space coordinate X. The $|\Delta T(X)|$ curve (solid line) was computed using the sampling theorem and normal data, d = 171 Å, with phases (−, +, −, +, −, +) for regions I, II, III, IV, V, and VI. The Fourier transform values of normal myelin are indicated by open circles (o), while the corresponding values for myelin swollen in 6.5% glycerol are indicated by small black dots (·).

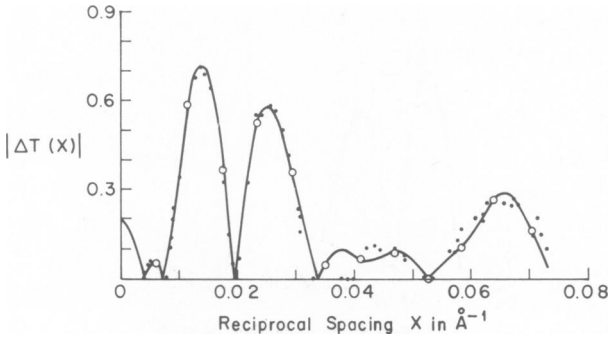

FIGURE 11 The modulus of the continuous transform $|\Delta T(X)|$ plotted vs. reciprocal space coordinate X. The $|\Delta T(X)|$ curve (solid line) was computed using the sampling theorem and normal data, d = 171 Å, with phases (−, +, −, +, +, −) for regions I, II, III, IV, V, and VI. The Fourier transform values of normal myelin are indicated by open circles (○), while the corresponding values for myelin swollen in 6.5% glycerol are indicated by small black dots (·).

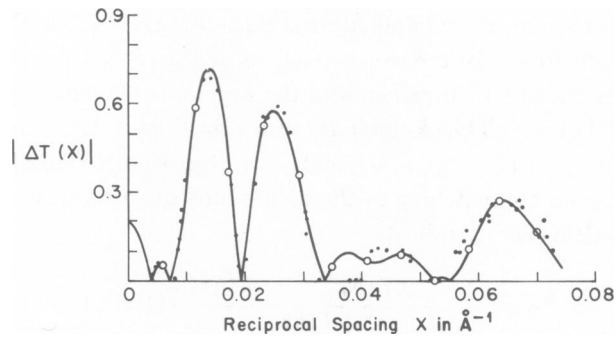

FIGURE 12 The modulus of the continuous transform $|\Delta T(X)|$ plotted vs. reciprocal space coordinate X. The $|\Delta T(X)|$ curve (solid line) was computed using the sampling theorem and normal data, d = 171 Å, with phases (−, +, −, +, +, +) for regions I, II, III, IV, V, and VI. The Fourier transform values of normal myelin are indicated by open circles (○), while the corresponding values for myelin swollen in 6.5% glycerol are indicated by small black dots (·).

TABLE III

RE VALUES FOR EACH PHASE CHOICE IN REGIONS V AND VI

Region:	Phases V	Phases VI	RE values
			%
	−	−	6.7
	−	+	7.1
	+	−	8.6
	+	+	9.2

continuous transform $\Delta T(X)$ computed from Eq. 7 and sampled at the observed data points, and where the summation is over all observed data points. Note that the R-equivalent index has similarity to the R-value of X-ray crystallography but there are differences so that we use the term RE. The RE values for the four phase choices for regions V and VI are listed in Table IV. The smallest RE value is for the (−, −) phase choice for regions V and VI and, provided that the differences in the RE values are significant, this phase choice is very likely to be correct.

VALIDITY OF PHASE CHOICE

The AI values in Table II and the sampling theorem reconstructions in Figs. 7 and 8 provide definitive evidence for assigning a (+) phase to region IV. The assignment of phases to regions V and VI are not as definitive and depends on whether the differences in AI values in Table II are real and whether the differences between RE values in Table III are real. Arguments are presented that these differences are, in fact, real so that the phase choice (−, −) for regions V and VI is correct. It is convenient to refer to the phase choice of (+, −, −) as the first choice for regions IV–VI and to refer to the phase choice of (+, −, +) as a possible second choice. These two phase choices are listed in Table IV in terms of h = 6–12 orders of normal nerve and the corresponding phases for the 12-parameter model are included, for comparison.

The differences between AI values are comparatively small (0.5–1.1%) for the three different sets of data listed in Table II. These small differences arise from the fact that the higher-order diffraction only has a moderate effect on the autocorrelation function compared with the more intense first five orders. The experimental error in intensity measurement is 3–4% for the low orders of diffraction but is about 10% for the higher orders of diffraction. The estimated experimental error in intensity measurement corresponds to an AI value of 0.5–0.6%. Thus the differences in AI values are significant compared with experimental uncertainty.

It might be expected that the first phase choice for regions IV–VI would have an AI value equal to the experimental error of 0.5–0.6%. But the AI values in Table II approach a limiting value of 5%. This is because the X-ray data have a limited resolution of 7 Å and also the solution $s(x)$ is an approximation to the true solution. To perform the calculations, the solution $s(x)$ is divided into small finite strips of 4 Å in

TABLE IV

PHASES FOR THE DIFFRACTION ORDERS h = 6–12 OF NORMAL NERVE*

	$h = 6$	7	8	9	10	11	12
12-Parameter model	+	+	−	0	−	−	−
First choice	+	−	−	0	−	−	−
Second choice	+	−	−	0	+	+	+

*h = 6 occurs in region IV; h = 7, 8 occur in region V; h = 10, 11, 12 occur in region VI.

width and each strip has uniform density. These small errors derived from the computational procedures tend to a constant value of 5% and do not favor any particular phase choice. Note that in the study of the low-order phases of nerve myelin (McIntosh and Worthington, 1974) the magnitude of the limiting AI value for the low-order phase was verified by running a trial problem.

From the above considerations it is very likely that the differences between AI values in Table II are real. Moreover, the AI values obtained for the three different sets of X-ray data are consistent in that the smallest values correspond to the first phase choice in each case. The likelihood that the AI differences are real is considerably strengthened when the three sets of X-ray data are considered together.

The sampling theorem reconstructions in Figs. 7 and 8 show that the experimental data points fit much closer to the transform which is computed using a (+) phase for region IV. Therefore, the choice of a (+) phase for region IV is correct. Furthermore both the deconvolution and reconstruction results indicate that region IV has a (+) phase so that the phase of region IV is firmly established.

The sampling theorem reconstructions computed using the four phase choices for regions V and VI together with the phases (−, +, −, +) for regions I–IV are shown in Figs. 9–12. It is easy to see that the first and second phase choices in Figs. 9 and 10 lead to transforms which are closer to the experimental data points. Moreover, the differences between the transforms in Figs. 9 and 10 and the transforms in Figs. 11 and 12 are much greater than the experimental uncertainty in the data points. The RE values listed in Table III verify that the first phase choice (+, −, −) for regions IV–VI has the smallest value of 6.7% and is likely to be correct. The second phase choice has the next smallest value of 7.1% and is clearly preferred over the other two choices.

The deconvolution and reconstruction methods are two different ways of solving the phase problem of the higher-order diffraction of nerve. Moreover, the AI values and the RE values are not the same. The AI values measure how closely the autocorrelation function of the various phase choices fit the observed autocorrelation function derived from the experimental data. The autocorrelation function is the Fourier transform of the continuous diffracted intensity and is expressed in real space coordinates. The RE values measure how closely the experimental diffracted amplitudes fit the computed continuous Fourier transform. The transform values are expressed in reciprocal space coordinates.

In summary, two different direct methods of structure analysis have been applied to the higher-order diffraction data of nerve myelin. The results of the two different methods both indicate that the first phase choice (+, −, −) for regions IV–VI is correct. The phase choice of (+, −) for regions IV and V is firmly established. However, it is, at present, very difficult to determine that our choice of a (−) phase for region VI is correct as there is a small possibility that region VI might have a (+) phase. Nevertheless, the observed minimum in the AI values and the observed minimum in the RE values represent direct objective evidence favoring the phase choice (+, −, −) for regions IV–VI.

ELECTRON DENSITY SCALE IN ELECTRONS PER CUBIC ANGSTROM

An absolute electron density scale in electrons per cubic angstrom for nerve myelin has been previously given (Worthington and Blaurock, 1969; McIntosh and Worthington, 1974). The low-angle X-ray data of normal nerve and of nerve swollen in glycerol solutions were used to compute Fourier syntheses. The Fourier syntheses of the individual membranes superimposed almost exactly but the fluid layers were at different levels. Assignment of the electron densities to these levels provided an electron density scale in electrons per cubic angstrom. The present scale is identical to the one given previously (McIntosh and Worthington, 1974).

The Fourier synthesis of frog sciatic nerve using the first phase choice (−, +, +, −, −, +, −, −, 0, −, −, −) for the first 12 orders of d = 171 Å is shown in Fig. 13 together with the electron density scale in electrons per cubic angstrom. Note that this Fourier profile which was computed using the X-ray data from normal nerve shown in Fig. 3 is slightly different from an earlier Fourier synthesis (Worthington and McIntosh, 1973) as more accurate data has since been obtained. The nerve membrane profile is asymmetrical with a higher peak density of 0.386 electrons/Å on the cytoplasmic side of the membrane. The cytoplasmic high-density layer shows two peaks at $x \approx 9$ Å and $x \approx 21.5$ Å while the extracellular high-density layer shows only one definite peak at $x \approx 56.5$ Å. The two peaks on either side of the low-density regions at $x \approx 21.5$ Å and at $x \approx 56.5$ Å have about the same electron density value of 0.368 electrons/Å^3. The low-density region appears as a uniform strip of low electron density. The flat central region of low density is about 20 Å wide and has an average electron density of about 0.270 electrons/Å^3. The two peaks at $x \approx 21.5$ Å and at $x \approx 56.5$ Å define a region of the membrane about 45 Å in width which is approximately

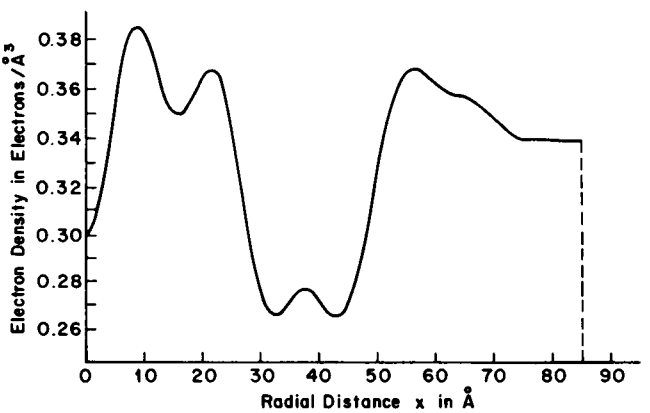

FIGURE 13 Fourier series representation of normal frog sciatic nerve myelin, d = 171 Å, for phase choice (−, +, −, +, −, −) for regions I, II, III, IV, V, and VI. An absolute electron density scale in electrons per cubic angstrom is included.

symmetrical about its center. The asymmetry of the nerve membrane is due to the higher density of the outer surface layer on the cytoplasmic side of the membrane.

In a previous paper (McIntosh and Worthington, 1974) evidence was presented in support of the existence of cytoplasmic and extracellular fluid layers between the individual nerve membranes. The cytoplasmic fluid layer is centered at $x = 0$ and the extracellular fluid layer is centered at $x = d/2$. Although the identification of molecular features directly from a Fourier synthesis is not rigorous as noted earlier (Worthington 1969 *b*) nevertheless the following points are noted. The Fourier synthesis shows a flat portion in the vicinity of $d/2$ with an electron density of about 0.338 electrons/Å^3 (which is the electron density of Ringer's solution). This flat portion implies the existence of an extracellular fluid layer. In the deconvolution analysis the choice of $\nu \approx 160$ Å means that the extracellular fluid layer is estimated to be about 11 Å wide. In Fig. 13 the cytoplasmic fluid layer is not shown as clearly or as definite as the extracellular fluid layer due to the limited resolution but the dip in electron density in the vicinity of $x = 0$ could imply the presence of a cytoplasmic fluid layer. The nerve myelin membrane in Fig. 13 is about 75 Å in width. This value is the same as obtained from model-building considerations (Worthington and King, 1971).

MOLECULAR INTERPRETATION

Nerve myelin contains about 80% lipid and 20% protein in terms of the dry weight (O'Brien, 1967). The cholesterol, glycerolipids, and sphingolipids in nerve myelin occur in an approximate molar ratio of 8:7:5 (O'Brien, 1967). Moreover, the lipid composition for peripheral nerve shows little variation for different kinds of nerves (O'Brien, 1967; Mokrasch, 1969). The protein components of peripheral nerve have been recently studied and they contain about 20% basic proteins and about 50–60% P_0 proteins (Eylar, 1973; Greenfield et al., 1973). The basic proteins refer to the A_1 and P_2 proteins (Eylar, 1973) and they occur in variable amounts in different sciatic nerves (Greenfield et al., 1973). Thus, it would appear that the main differences between sciatic nerves from different sources is in the distribution of the protein components.

The lipid molecules in nerve myelin are relatively long, some have as many as 26 CH_2 units in the hydrocarbon chain. The glycerolipids and sphingolipids have an average of about 20 CH_2 units per chain (O'Brien, 1967; Mokrasch, 1969). The length of an extended molecule of this average lipid is about 38 Å where the ionic head group and the methyl groups occupy a length of 13 Å. A classical extended lipid bilayer made solely from these hypothetical lipid molecules is 76 Å wide whereas the width of the nerve myelin membrane of frog sciatic nerve is 75 Å. This classical extended lipid bilayer is therefore an unsatisfactory model for nerve myelin as it leaves no room for assigning the protein components to the outside of the bilayer.

It is tempting to directly identify certain peaks in the Fourier synthesis with phosphate groups, cholesterol molecules, or some other molecular parameters. However, this procedure is invalid for a limited resolution Fourier synthesis (Worthington,

1969 *b*; Worthington, 1971) as such a synthesis contains a ripple contour due to series termination errors. It is recognized that the Fourier synthesis is an approximation to the true electron density profile of the unit cell and, consequently, the Fourier synthesis can only be used to give a general description of the distribution of molecular components within the membrane. This description can be expressed in terms of electrons per cubic angstrom when an absolute electron density scale for the Fourier synthesis is obtained as in Fig. 13.

From Fig. 13, the following general description of the molecular components can be given. The Fourier synthesis shows a symmetric bilayer part of about 45 Å in length and the uniform low-density region in the middle of this symmetric part is only about 20 Å in length. It is therefore likely that the nerve myelin membrane contains a symmetric lipid bilayer with lipid hydrocarbon chains which interdigitate in the uniform low-density region. A similar molecular arrangement was proposed in 1971 (Worthington, 1971). This earlier study made use of the phases of the 12-parameter model and these phases are the same as the first phase choice in Table IV apart from the weak $h = 7$ reflection. Thus, the Fourier synthesis derived from the 12-parameter model and the Fourier synthesis in Fig. 13 resemble each other. The molecular arrangement derived from model-building considerations is a symmetric lipid bilayer with interdigitating lipid hydrocarbon chains in the uniform low-density region of about 20 Å in width. The cholesterol molecules are equally distributed on each side of the membrane and pack closely to the lipid hydrocarbon chains which are closest to the ionic head groups. The tail portion of the cholestrol molecules may project into the narrow region of uniform low density. The width of this lipid bilayer is about 65 Å. Since the lipid hydrocarbon chains of the bilayer interdigitate, the width of this bilayer is less than the 76 Å width of the classical bilayer made from an average myelin lipid molecule. The molecular arrangement for the symmetric lipid bilayer is thought to apply to nerve myelin as it is in agreement with the Fourier synthesis of Fig. 13 and is also consistent with the electron scale in electrons per cubic angstrom.

The location of the protein components in peripheral nerve has not been determined. However, it would appear that the protein components in peripheral nerve are likely to be on either side of the symmetric lipid bilayer, either penetrating into the bilayer, or simply on the surface. The asymmetry in the Fourier profile in Fig. 13 is accounted for by assigning extra protein material to the cytoplasmic side of the membrane. The basic proteins are likely to be found on the outside of the lipid bilayer (Dickinson et al., 1970) while the P_0 proteins which have hydrophobic residues (Eylar, 1973) could be either on the outside or embedded into the lipid bilayer part of the membrane.

COMPARISONS BETWEEN THE TWO PHASE CHOICES

Fourier series representations for nerve myelin are computed using Eq. 2 and using the first and second phase choices in Table IV for the first 12 orders of diffraction. The first 12 diffraction orders from frog sciatic nerve $d = 171$ Å and from rabbit sciatic nerve $d = 179$ Å are used in order to make comparisons between the phase choices. The

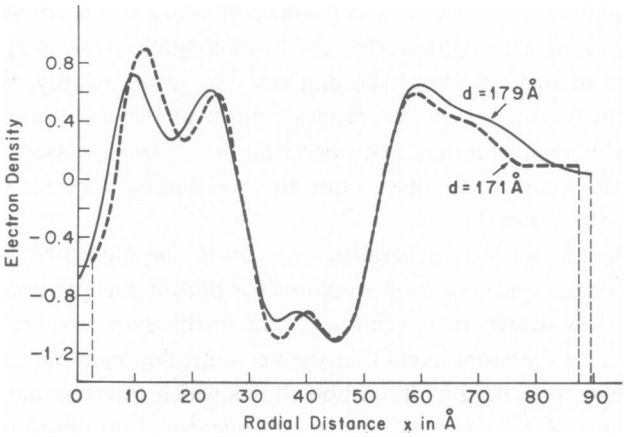

FIGURE 14 Fourier series representations of normal frog sciatic nerve myelin, d = 171 Å (dotted curve), and normal rabbit sciatic nerve myelin, d = 179 Å (solid curve), for phase choice (−, +, −, +, −, −) for regions I, II, III, IV, V, and VI.

phase choices in Table IV refer specifically to frog sciatic nerve but the swelling data from rabbit sciatic nerve[2] tend to resemble the X-ray data shown in Figs. 2–4 and hence it is reasonable to assume that the sciatic nerves of rabbit and frog have the same phases.

The Fourier series representations of rabbit and frog sciatic nerves computed using the first phase choice are shown in Fig. 14. The Fourier profiles have about the same resolution: 7 Å for frog nerve and 7.5 Å for rabbit sciatic nerve. The nerve membrane profiles tend to superimpose provided that the origin of the frog electron density profile is shifted 2.5 Å relative to the origin of the rabbit electron density profile. The central low-density regions of frog and rabbit sciatic nerves have a very similar shape and width. There is a definite symmetric part on either side of the central low-density region and this symmetric part is about 45 Å in length. The overall width of the rabbit nerve membrane is slightly wider than the frog nerve membrane by about 1 Å on the cytoplasmic side and about 1 Å on the extracellular side. The cytoplasmic fluid layer centered at $x = 0$ is 5 Å wider in the rabbit nerve than in the frog nerve.

The Fourier series representations of frog and rabbit sciatic nerve computed using the second phase choice are shown in Fig. 15. The Fourier profiles have the same resolutions as the profiles in Fig. 14. In order to obtain the best overlap between curves the origin of the frog electron density profile is shifted 2.5 Å relative to the origin of the rabbit electron density profile. The central low-density regions of rabbit and frog sciatic nerves have a similar shape and have about the same width but this width of overlap is only about 10 Å. Moreover, the low-density region for the frog nerve appears to be a little narrower than the corresponding region for the rabbit nerve. There is no symmetric part on either side of the low density regions. The overall width of

[2]McIntosh, T. J., and C. R. Worthington. Unpublished data.

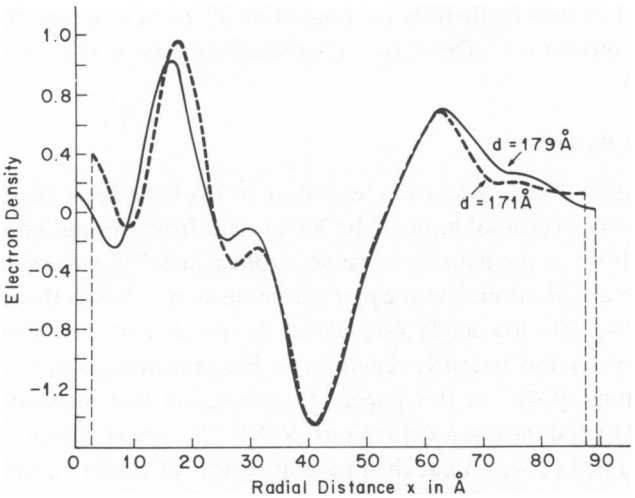

FIGURE 15 Fourier series representations of normal frog sciatic nerve myelin, d = 171 Å (dotted curve), and normal rabbit sciatic nerve myelin (solid curve), for phase choice (−, +, −, +, −, +) for regions I, II, III, IV, V, and VI.

the rabbit nerve membrane is slightly wider than the frog nerve membrane by about 1 Å on both sides. The cytoplasmic fluid layer is 5 Å wider in the rabbit nerve than in the frog nerve.

A molecular model for the symmetric bilayer part of Fig. 14 has been described. The close matching of the central low-density regions of the profiles for frog and rabbit sciatic nerves in Fig. 14 contrasts with the poorer matching of the corresponding regions in Fig. 15. By comparison, Caspar and Kirschner (1971) described a large mismatch of 3 Å between the low-density regions of rabbit and sciatic nerves. However, the close matching of the low-density regions is to be anticipated as the lipid composition of nerve myelin shows little variation between the different peripheral nerves (O'Brien, 1967; Mokrasch, 1969). Differences in the protein components of frog and rabbit sciatic nerves are to be expected (Eylar, 1973) and some differences between the two profiles in Fig. 14 at the outer surfaces of the two membranes are present.

It is clear that the assemblies of membrane components corresponding to the first and second phase choice are quite different. The Fourier synthesis of Fig. 15 indicates an extremely narrow membrane yet with a central region of very low electron density. The high-density peaks are separated by about 45 Å. If, it is assumed that these peaks correspond to ionic head groups, then the Fourier profile could be interpreted in terms of an asymmetric lipid bilayer of about 55 Å in width. The low-density regions are sharply defined and have similarity to the central low-density regions shown by some lipid bilayer systems, for example, cholesterol and egg lecithin (Levine and Wilkins, 1971). In the lipid bilayer systems the central dip in density is attributed to a marked localization of terminal methyl groups in the center of the bilayer (Levine and Wilkins, 1971; Levine, 1972). The location of protein components in the profile in Fig. 15 is

not known and moreover there is no suggestion of protein molecules on the outer surfaces of the membrane. The reason for the asymmetry of the lipid bilayer part is also not known.

DISCUSSION

Low-angle X-ray diffraction data at a resolution of 7 Å have been recorded from nerve myelin swollen in glycerol solutions. The X-ray data from normal nerve lie closely on the same transform as the data from nerve swollen in 6.5% glycerol and, hence, the molecular structure of the membrane pair at a resolution of 7 Å is the same for normal and swollen nerve. The low-angle X-ray data fall into six distinct regions of reciprocal space. The phases of the first three regions have been previously determined (McIntosh and Worthington, 1974). In this paper, deconvolution and reconstruction methods have been used to find the phases of regions IV–VI. The phase choice for these regions is very likely to be (+, −, −) but the phase of region VI is not completely settled so that an alternate choice of (+, −, +) may still be a possibility.

The observation that the higher-order X-ray data from swollen nerve fall into three distinct regions has led to a definite simplification of the phase problem of the higher orders. The $h = 6$ reflection of normal nerve is in region IV, the $h = 7$ and 8 reflections are in region V and have the same phases, while the $h = 10$, 11, and 12 reflections are in region VI and have the same phases. From Table I it can be seen that the previous phases are wrong. The phases derived from model-building considerations (Worthington and Blaurock, 1969; Worthington, 1969 *a*) have opposite phases for the $h = 7$ and 8 orders whereas the phases derived from symmetry considerations and Fourier comparisons (Caspar and Kirschner, 1971) have opposite phases for the $h = 7$ and 8 orders and the $h = 12$ reflection has an opposite phase from the $h = 10$ and 11 reflections. On the other hand, it can be seen from Table IV that the seven-parameter model and later versions (Worthington and King, 1971) have the same phases as the first phase choice apart from the $h = 7$ reflection.

It should be emphasized that the present analysis is based on many sets of low-angle X-ray diffraction data. In previous studies of the higher-order phase problem of nerve myelin only one or two sets of X-ray data were used. Worthington and King (1971) used two data sets, from normal and subnormal nerve, to obtain the phase of the $h = 6$ reflection while Caspar and Kirschner (1971) used two data sets, from rabbit sciatic and rabbit optic nerve, in their analysis. In the present study the various data sets for 0% glycerol, 6.5% glycerol, and 15% glycerol are plotted in Figs. 2, 3, and 4, respectively. It is this additional information provided by the many X-ray experiments which enables a phase solution to be obtained for the higher-order diffraction of nerve myelin.

The difficulty experienced in choosing the correct set of phases for the regions IV, V, and VI revolves around trying to show that the differences in AI and RE values are significant. These differences are of necessity small as the X-ray intensities of the higher-order reflections are weak compared with the intensities of the lower orders.

However, one set of phases, the first phases choice in Table IV, has the smallest AI and RE values and two other sets of swelling data show AI values which also indicate that this phase choice is very likely to be correct. Whether this first phase choice is, in fact, correct or not is very difficult to answer but definite and objective evidence has been obtained which is in support of the first phase choice.

A molecular model for the symmetric bilayer part of the Fourier profile computed using the first phase choice has been described. This symmetric lipid bilayer model has the lipid hydrocarbon chains interdigitated and the cholestrol molecules are uniformly distributed on each side of the bilayer. The protein distribution accounts for the asymmetry of the nerve membrane profile. On the other hand, the molecular description of the Fourier profile computed using the second phase choice is quite different.

This work was supported by a grant from the U. S. Public Health Service.

Received for publication 13 February 1974 and in revised form 17 May 1974.

REFERENCES

BLAUROCK, A. E. 1971. *J. Mol. Biol.* **56**:35.
BLAUROCK, A. E., and C. R. WORTHINGTON. 1969. *Biochim. Biophys. Acta.* **173**:419.
CASPAR, D. L. D., and D. A. KIRSCHNER. 1971. *Nat. New Biol.* **231**:46.
DICKINSON, J. P., K. M. JONES, S. R. APARICIO, and C. E. Lumsden. 1970. *Nature (Lond.).* **227**:1132.
ENG, L. F., F. C. CHAO, B. GERSTL, D. PRATT, and M. G. Tavaststjerna. 1968. *Biochemistry.* **7**:4455.
EYLAR, E. H. 1973. *In* Proteins of the Nervous System. D. J. Schneider, R. H. Angeletti, R. A. Bradshaw, A. Grasso, and B. W. Moore, editors. Raven Press, New York.
FINEAN, J. B. 1969. *Q. Rev. Biophys.* **2**:1.
FINEAN, J. B., and R. E. BURGE. 1963. *J. Mol. Biol.* **7**:672.
FLETCHER, R., and C. M. REEVES. 1964. *Comput. J.* **7**:149.
GREENFIELD, S., S. BROSTOFF, E. H. EYLAR, and P. MORELL. 1973. *J. Neurochem.* **20**:1207.
HOSEMANN, R., and S. N. BAGCHI. 1962. Direct Analysis of Diffraction by Matter. North-Holland Publishing Co., Amsterdam.
KING, G. I. 1971. Ph.D. Thesis. University of Michigan.
KING, G. I., and C. R. WORTHINGTON. 1971. *Phys. Letters.* **35A**:259.
LESSLAUER, W., J. E. CAIN, and J. K. BLASIE. 1972. *Proc. Natl. Acad. Sci. U.S.A.* **69**:1499.
LEVINE, Y. K. 1972. *Prog. Biophys. Mol. Biol.* **24**:1.
LEVINE, Y. K., and M. H. F. WILKINS. 1971. *Nat. New Biol.* **230**:69.
LONDON, Y. 1971. *Biochim. Biophys. Acta.* **249**:188.
LONG, C., editor. Biochemists' Handbook. 1961. Van Nostrand Reinhold, New York.
MCINTOSH, T. J., and C. R. WORTHINGTON. 1974. *Biophys. J.* **14**:363.
MOKRASCH, L. C. 1969. *In* Handbook of Neurochemistry. A. Lajtha, editor. Plenum Press, New York.
MOODY, M. F. 1963. *Science (Wash. D.C.).* **142**:1173.
O'BRIEN, J. S. 1967. *J. Theor. Biol.* **15**:307.
SCHMITT, F. O., R. S. BEAR, and G. L. CLARK. 1935. *Radiology.* **25**:131.
SCHMITT, F. O., R. S. BEAR, and K. J. PALMER. 1941. *J. Cell Comp. Physiol.* **18**:31.
SHANNON, C. E. 1949. *Proc. IRE.* **37**:10.
SHIPLEY, G. G. 1973. *In* Biological Membranes. Vol. II. D. Chapman, editor. Academic Press, Inc., New York.
WORTHINGTON, C. R. 1969 *a. Proc. Natl. Acad. Sci. U.S.A.* **63**:604.
WORTHINGTON, C. R. 1969 *b. Biophys. J.* **9**:222.

WORTHINGTON, C. R. 1971. *In* Biophysics and Physiology of Excitable Membranes. W. J. Adelman, editor. Van Nostrand Reinhold Company, New York.
WORTHINGTON, C. R. 1972. *Ann. N.Y. Acad. Sci.* **195**:293.
WORTHINGTON, C. R. 1973. *Curr. Top. Bioenerg.* **5**:1.
WORTHINGTON, C. R., and A. E. BLAUROCK. 1968. *Nature (Lond.).* **218**:87.
WORTHINGTON, C. R., and A. E. BLAUROCK. 1969. *Biophys. J.* **9**:970.
WORTHINGTON, C. R., and G. I. KING. 1971. *Nature (Lond.).* **234**:143.
WORTHINGTON, C. R., G. I. KING, and T. J. MCINTOSH. 1973. *Biophys. J.* **13**:480.
WORTHINGTON, C. R., and T. J. MCINTOSH. 1973. *Nat. New Biol.* **245**:97.

APPENDIX I: TREATMENT OF DIFFUSE REFLECTIONS

A brief account of the theory of intensity measurement is presented. Let $g(x)$ define an assembly of N unit cells:

$$g(x) = t(x) * \phi(x), \tag{11}$$

where $\phi(x)$ is an assembly of N lattice points. $G(X)$ and $\Phi(X)$ are Fourier transforms of $g(x)$ and $\phi(x)$, respectively. Thus, the diffracted intensity $|G(X)|^2$ is given by

$$|G(X)|^2 = J(X)\Phi^2(X), \tag{12}$$

where $\Phi^2(X)$ is the interference function. The total integrated intensity Ω is given by

$$\Omega = \int_{-\infty}^{\infty} |G(X)|^2 dX, \tag{13}$$

and Ω is the total area under the densitometer tracing. The treatment of intensities can be derived from Pareval's theorem:

$$\int_{-\infty}^{\infty} |G(X)|^2 dX = \int_{-\infty}^{\infty} g^2(x)dx. \tag{14}$$

Now as each unit cell $t(x)$ cannot overlap, it follows that

$$\int_{-\infty}^{\infty} g^2(x)dx = N \int_0^d t^2(x)dx \tag{15}$$

for any $\phi(x)$. Thus the value of Ω is a constant and the value of Ω is not dependent on the interference function.

In an X-ray swelling experiment as the adjacent membrane pairs are separated by fluid spaces of 30–100 Å in width, a small variation in this width is likely to occur. Thus, swollen nerve shows discrete lower-order reflections but the higher-order reflections become broader and overlap and occur as diffuse reflections. From the above theory the correct procedure is to measure the total area under the densitometer tracing. This total area Ω is independent of the disorder in the system. If no disorder was present in the assembly, the discrete reflections are recorded and Ω is the area under the densitometer tracing belonging to the discrete reflec-

tions. If the assembly of unit cells had random order, then Ω is simply N times $\int_{-\infty}^{\infty} J(X)dX$. In the general case when there is partial disorder in the system the lower orders of diffraction are discrete, but the higher orders of diffraction overlap and appear diffuse. The transition from discrete reflections to diffuse reflections depends on the amount of disorder in the system (Hosemann and Bagchi, 1962). However, no matter what the value of the interference function, the diffracted intensity $|G(X)|^2$ will show the zeroes of $J(X)$ as $|G(X)|^2$ is obtained from a multiplication of $J(X)$ and $\Phi^2(X)$. When there is partial disorder in the assembly, the intensities of the discrete reflections of period d are measured in the usual way. The intensities of the diffuse reflections are obtained by choosing the period d of the discrete reflections as the sampling interval so that a set of equivalent integrated intensities is obtained by measuring the areas under the densitometer curve for the sampling intervals (h/d). This procedure allows the experimental data points to be put on a relative scale.